applied sciences

MDPI

Article

Assessing Ground Motion Intensity Measures and Structural Damage Measures in Underground Structures: A Finite Element Analysis of the Daikai Subway Station

Tong Liu [1], Yulong Han [2], Qinghe Wang [2,*] and Yong Yuan [3]

[1] School of Management, Shenyang Jianzhu University, Shenyang 110168, China; ltharmony@163.com
[2] School of Civil Engineering, Shenyang Jianzhu University, Shenyang 110168, China; hylyjs@163.com
[3] State Key Laboratory of Disaster Reduction in Civil Engineering, Tongji University, Shanghai 200092, China; yuany@tongji.edu.cn
* Correspondence: wangqinghe@sjzu.edu.cn; Tel.: +86-(0)24-2469-1868

Abstract: Research on the characterization of ground motion intensity and damage of underground structures is limited, while reasonable selection of ground motion intensity measures and structural damage measures is a crucial prerequisite for structural seismic performance evaluation. In this study, a two-dimensional finite element model of soil and structures was established based on the Daikai subway station in Japan. Through incremental dynamic analysis, 32 ground motion intensity measures and seven structural damage measures were comprehensively evaluated from seven properties, including efficiency, practicality, proficiency, scaling robustness, relativity, hazard computability, and sufficiency. According to the analysis results, the purpose and significance of each property during measure optimization were hierarchically sorted out. The results show that peak ground acceleration, acceleration spectrum intensity, and sustained maximum acceleration are recommended as ground motion intensity measures, while maximum inter-story drift ratio, column end displacement angle, and two-parameter measures are recommended as the structural damage measures for seismic performance evaluation of the shallow-buried subway station. Furthermore, measure optimization approaches are proposed as follows: the basic selection of IMs should satisfy scaling robustness, hazard computability, and sufficiency to site condition; the optimal selection of IMs is suggested to be evaluated mainly through efficiency, practicality and proficiency, and verified through relativity and relative sufficiency between IMs. The optimal selection of DM is suggested to be evaluated through four properties, including efficiency, practicality, proficiency, and relativity.

Keywords: subway station structure; ground motion intensity measure; structural damage measure; incremental dynamic analysis; measure optimization approach

check for updates

Citation: Liu, T.; Han, Y.; Wang, Q.; Yuan, Y. Assessing Ground Motion Intensity Measures and Structural Damage Measures in Underground Structures: A Finite Element Analysis of the Daikai Subway Station. *Appl. Sci.* **2024**, *14*, 5491. https://doi.org/10.3390/app14135491

Academic Editor: Muhammad Junaid Munir

Received: 16 November 2023
Revised: 1 June 2024
Accepted: 7 June 2024
Published: 25 June 2024

Copyright: © 2024 by the authors. Licensee MDPI, Basel, Switzerland. This article is an open access article distributed under the terms and conditions of the Creative Commons Attribution (CC BY) license (https://creativecommons.org/licenses/by/4.0/).

1. Introduction

The advancement of performance-based seismic design necessitates a comprehensive understanding of the relationship between ground motion inputs and the dynamic responses of underground structures. This has led to the growing utilization of incremental dynamic analysis (IDA) as a potent tool for evaluating the seismic performance of various underground constructions such as subway stations [1–5], tunnels [6,7], and underground cavern groups [8]. IDA offers the advantage of accounting for the randomness of seismic ground motion and the structural response characteristics under significant seismic events. Nevertheless, the accurate implementation of IDA relies heavily on the selection of appropriate ground motion intensity measures (IMs) and structural damage measures (DMs).

Prior research has made considerable strides in establishing criteria for the optimal selection of IMs and DMs when conducting IDA for underground structures. For example, Chen et al. [9] explored the relationship between IMs and DMs in the context of mountain

tunnels, revealing that IMs vary for different ground motion scenarios. Likewise, Kiani et al. [10] undertook an IDA on underground steel pipelines, assessing 23 distinct IMs based on parameters like efficiency, sufficiency, and scaling robustness. From this evaluation, they identified energy density and a composite measure of velocity and spectral velocity types as the most effective IMs. Further contributions have come from Zhong et al. [11], who assessed 22 IMs and four DMs with regard to the Daikai subway station in Japan in terms of efficiency, practicality, and proficiency, identifying acceleration-type IMs and maximum inter-story drift ratio as particularly relevant for seismic performance evaluations of this station. Zhuang et al. [3] investigated how different IMs affect the seismic fragility curves of the same station from efficiency, practicality, proficiency, and relativity, finding that peak ground acceleration (PGA) and peak relative lateral displacement are especially useful in this context. Similarly, Zhang et al. [7], Gu et al. [12], Huang et al. [13], and Jiang et al. [14] have provided valuable insights into the applicability of various IMs and DMs for circular tunnels, pipe galleries, and underground frame structures with different cross-sectional types, respectively. In summary, the study on optimal selection of IMs and DMs during IDA for underground structures has already made some progress; however, the types of IMs and DMs considered and the purpose as well as significance of different properties of the comprehensive evaluation approach during measure optimization must be clarified and improved further.

To fill this gap, the current study focuses on the Daikai subway station as a case study representative of shallow-buried underground structures. We evaluated 32 IMs—both scalar and vector types—and seven DMs, which include metrics related to displacement, energy, and two-parameter types. These measures were assessed based on seven essential criteria: efficiency, practicality, proficiency, scaling robustness, relativity, hazard computability, and sufficiency. The results were then systematically organized and hierarchically classified, laying the groundwork for developing a robust measuring system for future seismic evaluations of underground constructions.

2. Selection of IMs and DMs

The reasonable selection of IMs and DMs can significantly enhance the accuracy of IDA-based evaluations of seismic performance in structural engineering. Generally, IMs are categorized into scalar and vector types [15]. Scalar-type IMs are expressed using a single parameter, such as PGA, peak ground velocity (PGV), and spectral acceleration (S_a). Vector-type IMs are defined using two or more parameters, mitigating the risk of inaccuracies resulting from the limitations of a single parameter. In the context of this study, we considered 32 IMs, comprising 25 scalar and 7 vector types, which span various subcategories like acceleration, velocity, displacement, and spectral types [16,17]. Detailed specifications for these parameters are provided in Appendix A.

Currently, the division of seismic performance levels for underground structures is predominantly determined by the maximum inter-story drift ratio (θ_{max}) [18], adhering to criteria established for above-ground structures. However, this approach may not be fully appropriate due to the different load-transfer mechanisms that are a function of the surrounding soil in underground constructions. Therefore, this paper broadens the scope of DMs to encompass three dimensions: force, deformation, and energy. Specifically, we considered 7 DMs at both the structural layer and key component layer (such as the central column) to provide a more comprehensive understanding of the dynamic response characteristics of underground structures. In this respect, θ_{max}, energy ratio R_E, and two-parameter D_e are utilized as DMs at the structural layer. Meanwhile, column end displacement ratio θ_c, bending moment M_C, shear force F_{SC}, and axial force F_{NC} at the bottom of the central column are employed as DMs at the component layer.

The energy ratio R_{E} serves as a useful metric, representing the ratio of energy dissipated through structural plastic damage to the total energy input to the structure during seismic activity. The formal definition for this measure is as follows:

$$R_E = \frac{E_p^e}{\sum E_n} \tag{1}$$

where E_p^e represents the structural plastic damage energy dissipation; and $\sum E_n$ denotes the total input energy of the structure, including structural compression damage energy dissipation, structural plastic damage energy dissipation, and structural strain damage energy dissipation.

Furthermore, a two-parameter DM offers the advantage of accounting for the synergistic effects of both structural deformation and energy. In 1985, Park et al. [19] conducted an analysis on post-earthquake concrete column and beam elements, introducing a composite DM that combined deformation and hysteretic energy dissipation. This concept has since gained widespread acceptance. Subsequently, Jiang et al. [20] and Ou et al. [21] extended the two-parameter DM to masonry and steel structures, respectively. In the current study, we adapt this two-parameter concept to the seismic performance evaluations for underground structures. Specifically, we propose a linear combination measure based on inter-story displacement and R_{E}, aiming to assess its suitability for such structures. The definition for this measure is provided as follows:

$$D_{\mathrm{e}} = \frac{X_{\mathrm{m}}}{X_{\mathrm{u}}} + \frac{E_{\mathrm{p}}^{\mathrm{e}}}{\sum E_n} \tag{2}$$

where X_{m} stands for the maximum inter-story displacement of the structure; X_{u} signifies the maximum inter-story displacement corresponding to the collapse limit state of the structure, which can be obtained from reference [1], that is, the corresponding X_{u} is 0.0825 m.

3. Comprehensive Evaluation Properties and Implementation Procedures

In this section, we offer a detailed description of the seven-dimensional framework used for the comprehensive evaluation of IMs and DMs. We introduce the implementation steps necessary for selecting optimal IMs and DMs for shallow-buried underground structures, and, in doing so, establish a methodology for optimal measure selection.

Drawing on the logarithmic relationship between IMs and DMs as postulated by Cornell et al. [22], shown in Equation (3), we can evaluate the efficiency, practicality, and proficiency of the IMs and DMs through the fitting parameters a and b. Additionally, the sufficiency of these measures can be obtained through the fitting residual $\ln(\varepsilon \mid IM)$. The criteria for evaluating each property are elaborated upon as follows:

$$\ln(DM) = \ln(a) + b\ln(IM) + \ln(\varepsilon|IM) \tag{3}$$

3.1. Efficiency

Efficiency, as defined in the literature [23], implies that effective IMs and DMs can minimize the variability of the structural dynamic response for a given level of ground motion intensity. This, in turn, reduces the number of ground motion records needed for an accurate IDA. The logarithmic standard deviation β_{D} between IMs and DMs serves as the metric for assessing efficiency. A smaller β_{D} value indicates lower dispersion in structural dynamic response, and consequently, higher efficiency for the associated IMs and DMs. The formula to calculate β_{D} is given as follows:

$$\beta_D = \sqrt{\frac{\sum \left(\ln(DM) - \ln(aIM^b)\right)^2}{N-2}} \tag{4}$$

where a and b are the fitting parameters in Equation (3), and N is the total number of dynamic time history analyses. The specific meaning of β_D is expressed in Figure 1.

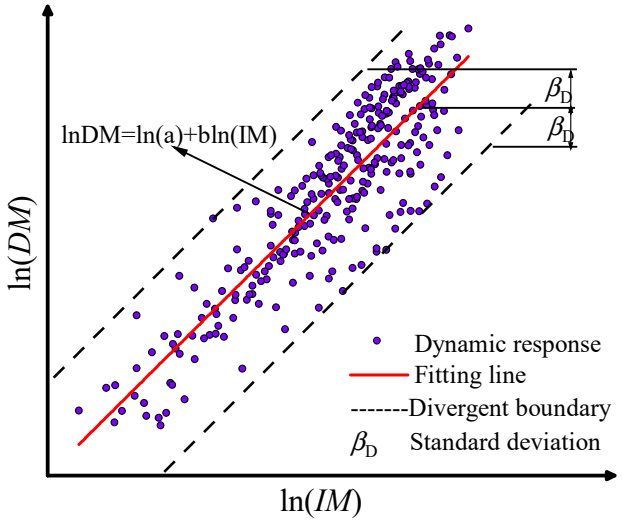


Figure 1. Schematic diagram of β_D.

3.2. Practicality

Practicality, as defined in previous research [24], is related to the sensitivity of the correlation between IMs and DMs. This sensitivity reflects how the amplitude modulation of ground motion affects the structural dynamic response. The linear regression coefficient b in Equation (3) is generally used for this assessment. The more significant the value of b, the more substantial the practicality of IM and DM, which indicate the more significant influence of ground motion amplitude modulation on the structural dynamic response, that is, with continuous increases in ground motion intensity, the whole process of the structural dynamic response from elastic, elastic–plastic, to collapse can be better captured.

3.3. Proficiency

Proficiency [25] is typically determined using the evaluation parameter ζ, as specified in Equation (5). The lower the value of ζ, the higher the proficiency of IMs and DMs. When efficiency and practicality cannot be simultaneously optimized, proficiency serves as a composite attribute that can be leveraged for a comprehensive evaluation, thereby reducing associated uncertainties.

$$\zeta = \frac{\beta_D}{b} \tag{5}$$

3.4. Scaling Robustness

Scaling robustness [26] implies that an IM is monotonic and can be proportionally adjusted. Concurrently, this adjustment should not introduce any bias in the results of the structural dynamic time history analysis. Typically, scaling robustness is assessed using the p-value derived from the F-test, with a significance level set at 5%. A higher p-value indicates a lower dependency of the structural dynamic response on the proportional adjustment factor, implying greater scaling robustness for the corresponding IM. Specifically, if the p-value exceeds 0.05, the slope of the regression line is near zero, affirming the scaling robustness of the IM. Conversely, a p-value of 0.05 or less negates this robustness. Given that scaling robustness also considers the impact of the adjustment factor on the structural dynamic response, and IMs and DMs satisfy the logarithmic distribution of Formula (3), ln(*DM*) and ln(Scale Factor) are used to assess IM scaling robustness when θ_{max} is the DM.

3.5. Relativity

Relativity [27] can be explored from two angles: the correlation between IMs and DMs, and the inter-correlation among different IMs. Typically, the statistical correlation

coefficient R^2 is used to determine this relationship. A higher R^2 value indicates a stronger correlation between the parameters under consideration. The formula for calculating R^2 is detailed below:

$$R^2 = \frac{SSR}{SST} = \frac{\sum(\overset{\bullet}{\ln} DM_i - \overline{\ln DM_i})^2}{\sum(\ln DM_i - \overline{\ln DM_i})^2} \quad (6)$$

where SST is the sum of squares for total, SSR represents the sum of squares for regression, $\overset{\bullet}{\ln} DM_i$ stands for the fitting structural damage logarithm, $\overline{\ln DM_i}$ indicates the average structural damage logarithm, and $\ln DM_i$ is the real structural damage logarithm.

3.6. Hazard Computability

Hazard computability [28] evaluates the feasibility of utilizing an IM for seismic hazard assessment. This involves employing probability models to calculate exceedance probabilities within specific time frames in a given region. The resulting hazard curves then serve as a basis for assessing the IM's hazard computability, focusing on both the simplicity of computation and the accuracy of the outcomes.

3.7. Sufficiency

Sufficiency [23] is a multi-faceted attribute, evaluated from two primary angles. First, the focus is on the sufficiency of the IM with respect to the site environment, including factors such as earthquake magnitude (M_W), epicenter distance (R_e), and fault distance (R). For this research, the sufficiency in terms of earthquake magnitude and fault distance is considered. A regression analysis of $\ln(\varepsilon \mid IM)$ against M_W and R is carried out, where ε denotes the residual. The p-value obtained from the F-test, at a 5% significance level, is used for this determination. A p-value less than or equal to 0.05 indicates that the IM is not sufficient; otherwise, it is deemed sufficient. Second, relative sufficiency between different IMs is examined, a methodology proposed by Jalayer et al. [29]. This uses the concept of relative entropy, as represented in Formula (7). A positive value of I suggests that IM_2 is more sufficient than IM_1, and the greater the value of I, the higher the sufficiency of IM_2. Conversely, a negative I implies greater sufficiency for IM_1.

$$I(DM|IM_2|IM_1) \approx \frac{1}{n}\sum \log_2\left[\frac{\beta_{D|IM_1}}{\beta_{D|IM_2}} \frac{\Phi(\ln(DM) - \ln(aIM_2{}^b)) \Big/ \beta_{D|IM_2}}{\Phi(\ln(DM) - \ln(aIM_1{}^b)) \Big/ \beta_{D|IM_1}}\right] \quad (7)$$

3.8. Implementation Procedures

The procedures for the optimal selection of IMs and DMs based on the aforementioned properties are summarized below, the technical route of this paper is depicted in Figure 2.

(a) Establish a finite element model of the soil and structures, considering site conditions and material properties, and validate its feasibility through existing literature data.
(b) Select an appropriate number of ground motions based on the site category and perform amplitude modulation.
(c) Implement the amplitude-modulated ground motions into the finite element model for IDA, extracting the IMs and DMs under study.
(d) Evaluate the seven properties discussed to determine the most suitable IM and DM for the structural system in question.
(e) Finally, each property's role in the evaluation process is identified, and an approach for the optimal selection of IMs and DMs is proposed.

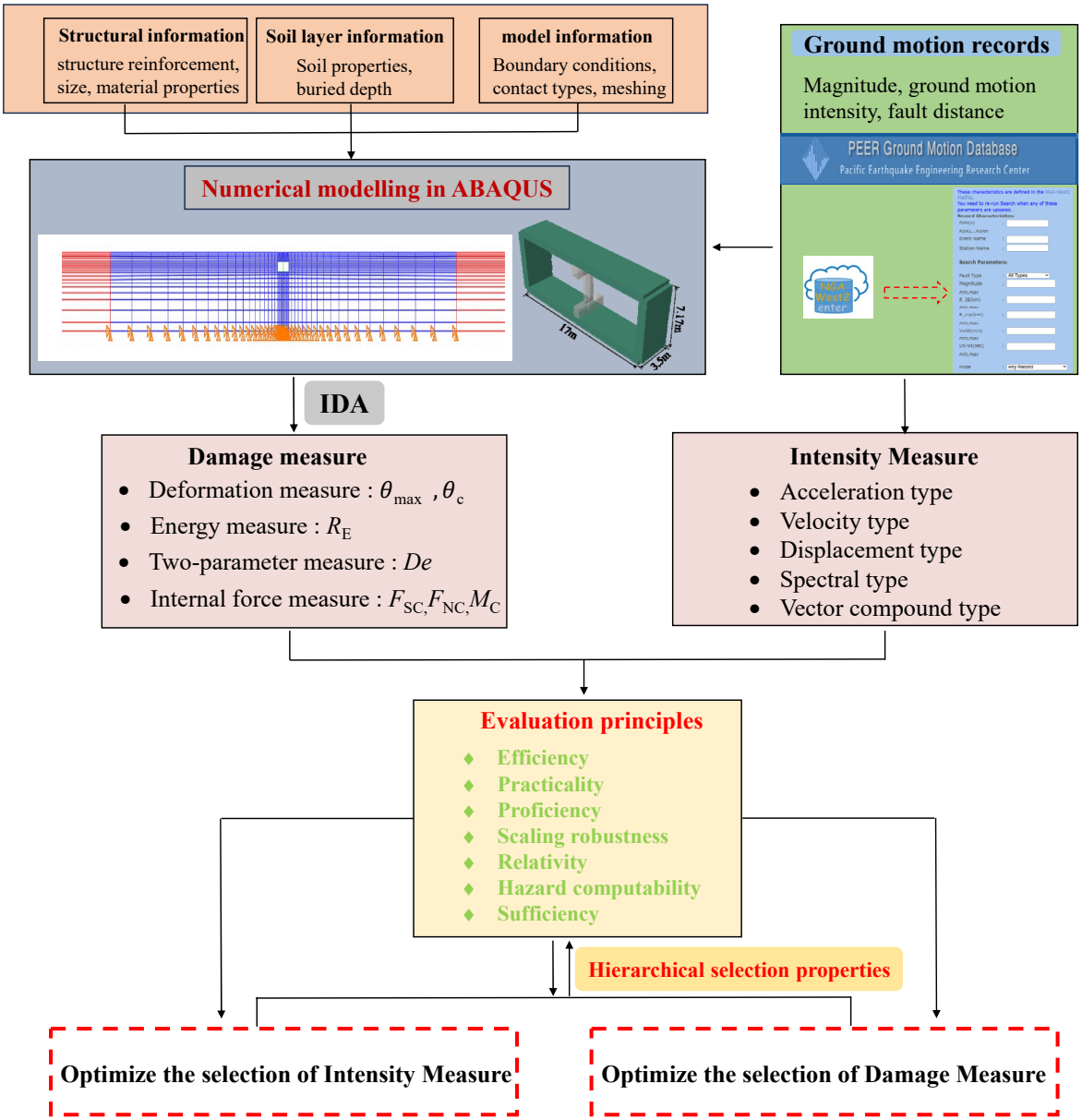


Figure 2. Comprehensive analysis of intensity and structural damage metrics.

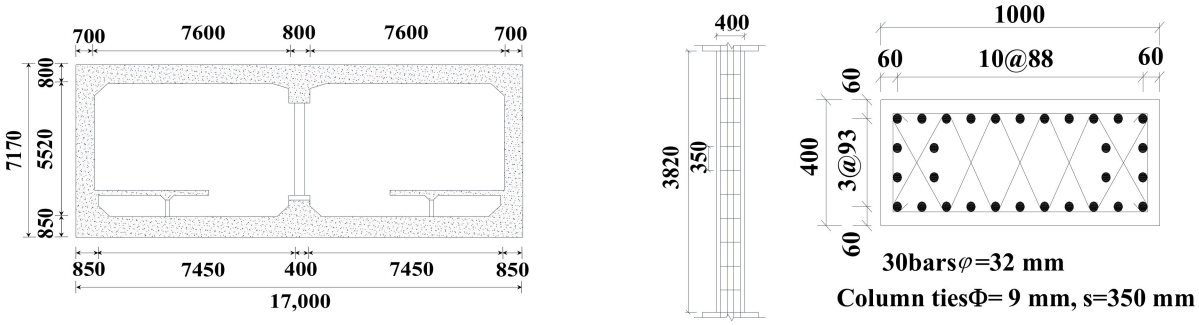
4. Numerical Example

4.1. Calculation Model

The primary focus of this study is on the Daikai subway station, severely damaged during the 1995 Kobe earthquake in Japan. Due to the significant impact of the earthquake damage and the comprehensive post-earthquake investigation, there is a substantial amount of actual damage data available, making it conducive to the corresponding research. As a result, this paper will adopt this case for its subsequent research efforts. The station's structural dimensions and reinforcement are depicted in Figure 3. Specifically, the structure has a cross-section measuring 17 m in width and 7.17 m in height. The center columns are longitudinally spaced at 3.5 m intervals, with a clear height of 3.82 m and cross-sectional dimensions of 0.4 m × 1.0 m. Figure 3b details the center column's reinforcement. The station is buried approximately 4.8 m underground, and the soil layer parameters for the site are provided in Table 1.

Due to its efficient nonlinear analysis capabilities, as well as a rich set of material and contact effect models, ABAQUS software (Abaqus 2022) is well suited for simulating the

mechanical characteristics of underground structures. Consequently, a two-dimensional finite element for both the soil and structures is established using ABAQUS software, as illustrated in Figure 4. This model extends 1000 m in length and rises 40 m in height. Beam element B21 is employed for structural simulation, while the plane strain element CPE4R is used for soil modeling.



(**a**) Cross-section of the Daikai subway station (**b**) Cross-section and reinforcement of the central column

Figure 3. Cross-section of the subway station and reinforcement details of the central column (mm).

Table 1. Soil parameters of the site of Daikai subway station.

No.	Soil Type	Depth (m)	Unit Weight (kN/m^3)	Cohesion Yield Stress (kPa)	Friction Angle (°)	Poisson's Ratio	Elastic Modulus (MPa)
1	Fill	0–1	19	20	15	0.33	101.308
2	Holocene sand	1–2	19	30	20	0.32	101.308
3	Holocene sand	2–4.8	19	1	40	0.32	147.840
4	Pleistocene clay	4.8–8	19	1	40	0.40	195.972
5	Pleistocene clay	8–17	19	30	20	0.30	290.342
6	Pleistocene clay soil	17–	20	1	40	0.26	560.045

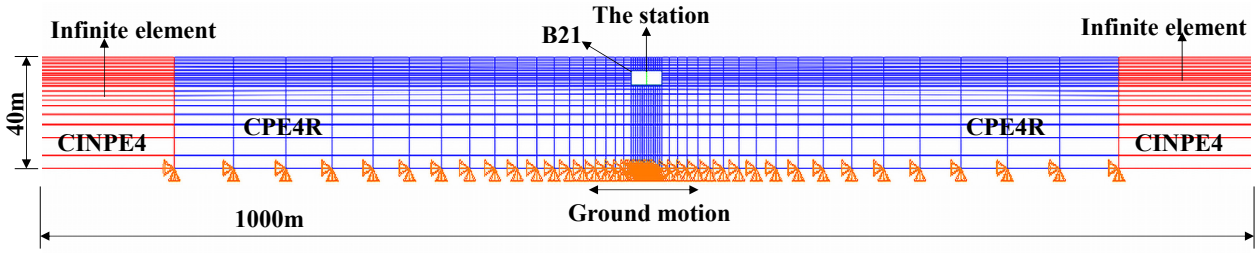


Figure 4. Numerical model of the structure and the surrounding soil.

The concrete's elastic–plastic behavior is modeled using the plastic damage model proposed by Lubliner et al. [30] and Lee et al. [31]. The concrete has a density of 25 kN/m^3 and an elastic modulus of 24 GPa. Reinforcement is implemented at the structural element level using the rebar command. Steel bars have a yield strength of 312 MPa and an elastic modulus of 200 GPa. The Mohr–Coulomb model is employed to account for the soil's elastic–plastic behavior. A frictional contact interface with a coefficient of friction (μ) of 0.4 is established between the soil and the structure. The top of the soil is free, while its bottom is fixed with both horizontal and vertical constraints. The ground motion is input horizontally at the bedrock.

To achieve more accurate calculations, the main structure is arranged in a dense, uniform 1 m × 1 m grid. The soil near the structure is densely arranged in a 1 m × 1 m grid to achieve precise dynamic responses. The remaining soil farther from the structure is discretized based on its distance, as illustrated in Figure 4.

Boundary conditions for the soil utilize infinite element CINPE4, and the analysis is executed in two stages. Initially, the structure is subjected to static calculations with

fixed horizontal and vertical constraints at the bottom. The structural model is statically calculated, the results of which are imported to achieve stress balance. Subsequently, these constraints are removed, and ground motions are introduced at the bedrock for dynamic implicit calculations. Due to the large size of the soil relative to the structure and the soil's energy dissipation, damping effects are considered negligible.

To validate the finite element model's accuracy, its dynamic responses during the Kobe earthquake are compared with analysis results from Huo et al. [32]. This comparison includes the central column's horizontal displacement and internal forces, as summarized in Table 2. All errors are within a 15% margin, affirming that the finite element model realistically captures the structure's dynamic characteristics and is suitable for further investigation.

Table 2. Verification of the finite element model of Daikai subway station.

Verify Indicators	Horizontal Displacement of Central Column (cm)	Maximum Axial Force (kN)	Maximum Shear Force (kN)	Static Axial Force (kN)
Results of Huo et al. [30]	3.8	4900	730	3700
Results of this study	3.41	4762.05	689.97	3205.68
Deviation (%)	10.26	2.82	5.48	13.36

4.2. The Selection of Ground Motion Records

Ground motion records for this study are primarily determined based on the site classification. According to the National Earthquake Hazards Reduction Program (NEHRP) guidelines [33], the shear wave velocity (V_s30) of the site where the Daikai station is located ranges from 180 m/s to 360 m/s. This categorizes the site as a Class D location. In terms of the number of ground motion records to be selected, the work by Shome and Cornell [34] suggests that a range of 10 to 20 records provides an adequate representation of ground motion randomness. Additionally, it has been observed that pulse-like ground motions, which contain numerous low-frequency components, induce significant structural dynamic responses. These responses manifest as variations in the internal force within the central column, lateral deformation of the soil layer, and displacement of the side walls. These effects are notably more pronounced compared to non-pulse motions [35,36]. Therefore, 18 pulse-like ground motion records were chosen for this study based on the multi-component velocity pulse identification method proposed by Shahi and Baker [37]. These records were sourced from the NGA-West2 strong earthquake database, part of the Pacific Earthquake Engineering Research (PEER) Ground Motion Database [38]. All selected records correspond to a Class D site, as detailed in Table 3. To comprehensively capture the structure's dynamic response, from elastic behavior through to elastic–plastic and finally to collapse during IDA, these 18 ground motion records were subject to amplitude modulation. Preliminary calculations showed initial amplitude modulations of PGA at 0.03 g, 0.06 g, and 0.1 g. These amplitudes were then incrementally adjusted up to 0.8 g in steps of 0.05 g.

Table 3. Eighteen pulse-like ground motion records.

No.	Event	Station	Mag. (M_W)	R (km)	Pulse Period (s)	V_s30 (m/s)	Direction	PGA (g)	PGV (cm/s)
1	Imperial Valley-06, 1979	El Centro Array #10	6.53	8.60	4.515	202.85	E10320	0.23	46.25
2	Superstition Hills-02, 1987	Parachute Test Site	6.54	0.95	2.394	348.69	PTS225	0.43	134.81
3	Loma Prieta, 1989	Saratoga-W Valley Coll	6.93	8.48	5.649	347.9	WVC270	0.33	64.94
4	Kobe, Japan, 1995	Takarazuka	6.9	0	1.806	312.00	TAZ090	0.61	86.27
5	Northridge-01, 1994	Pardee-SCE	6.69	5.54	1.232	325.67	PAR--T	0.30	53.97
6	Kobe, Japan, 1995	Takatori	6.9	1.46	1.554	256.00	TAK090	0.67	123.14

Table 3. *Cont.*

No.	Event	Station	Mag. (M_W)	R (km)	Pulse Period (s)	V_s30 (m/s)	Direction	PGA (g)	PGV (cm/s)
7	Chi-Chi, Taiwan, 1999	CHY101	7.62	9.94	5.341	258.89	CHY101-E	0.34	64.99
8	Chi-Chi, Taiwan, 1999	TCU038	7.62	25.42	9.576	297.86	TCU038-E	0.15	56.76
9	Imperial Valley-06, 1979	El Centro Array #6	6.53	0	3.773	203.22	E06230	0.45	113.61
10	Darfiel, New Zealand, 2010	HORC	7.00	7.29	9.919	326.01	HORCN18E	0.45	105.92
11	Darfield, New Zealand, 2010	ROLC	7.00	0	7.140	295.74	ROLCS29E	0.39	85.73
12	Imperial Valley-06, 1979	El Centro Differential Array	6.53	5.09	6.265	202.26	EDA270	0.35	75.46
13	Darfield, New Zealand, 2010	TPLC	7.00	6.11	8.932	249.28	TPLCN27W	0.29	76.32
14	Darfield, New Zealand, 2010	NNBS North New Brighton School	7.00	26.76	8.043	211.00	NNBSS13E	0.21	56.51
15	Chi-Chi, Taiwan, 1999	TCU059	7.62	17.11	7.784	272.67	TCU059-E	0.16	51.38
16	Imperial Valley-06, 1979	El Centro Array #7	6.53	0.56	4.375	210.51	E07230	0.47	113.15
17	Kobe, Japan, 1995	Port Island	6.90	3.31	2.828	198.00	PRI000	0.35	90.67
18	Denali, Alaska, 2002	TAPS Pump Station#10	7.90	0.18	3.157	329.40	PS10-047	0.33	115.71

5. Results and Analysis

5.1. Efficiency Analysis

Figure 5 provides an in-depth view of the efficiency for the 32 IMs and seven DMs considered in this study. Remarkably, the efficiency of each DM remains relatively consistent across different IM parameters. The β_D corresponding to F_{NC} is the lowest, followed by F_{SC}, M_C, and R_E, and finally D_e, θ_c, and θ_{max}. Notably, energy-type DMs outperform those based on displacement. In the context of IMs, acceleration-type IMs display relatively lower β_D values, signifying superior efficiency. Figure 6 showcases the β_D values for each IM when F_{NC} serves as the DM, elucidating the inferior efficiency of displacement-type IMs relative to their acceleration-type counterparts. A detailed comparative analysis of β_D for various IM types under each DM is depicted in Figure 7, which reveals that SMA, A_{rs}, Arias intensity, ASI, and PGA are the most efficient IMs. Furthermore, acceleration-type IMs outperform those based on displacement in efficiency, which is true for each DM considered herein.

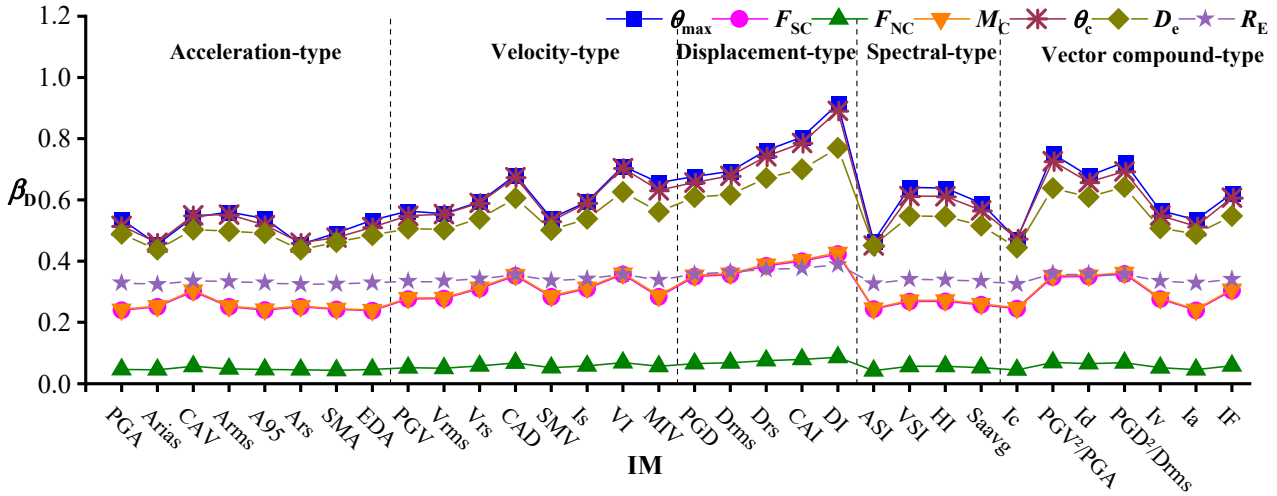


Figure 5. The value of β_D with different IMs and DMs.

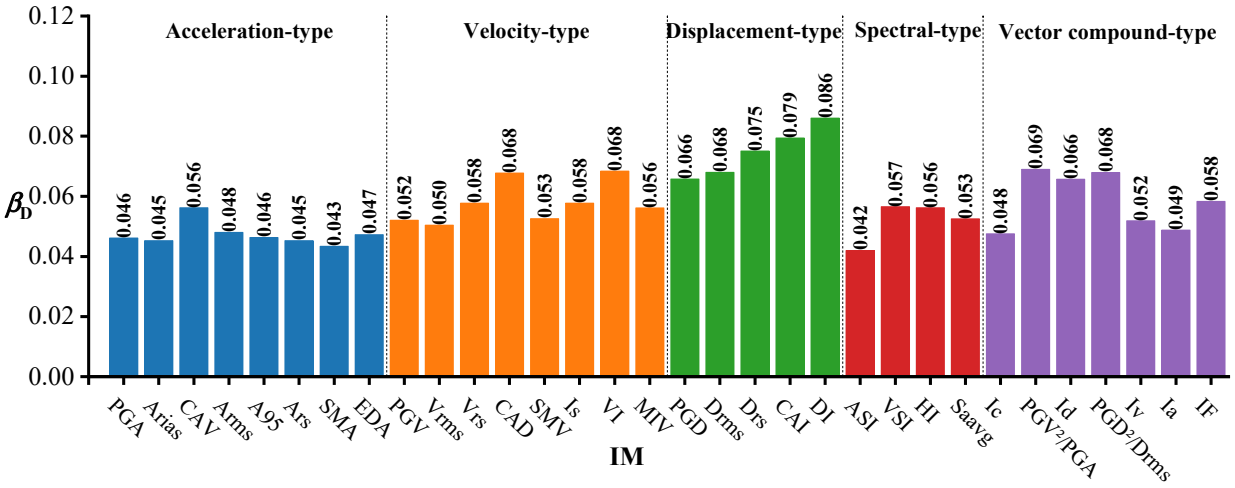


Figure 6. The value of β_D under each IM with F_{NC} as the DM.

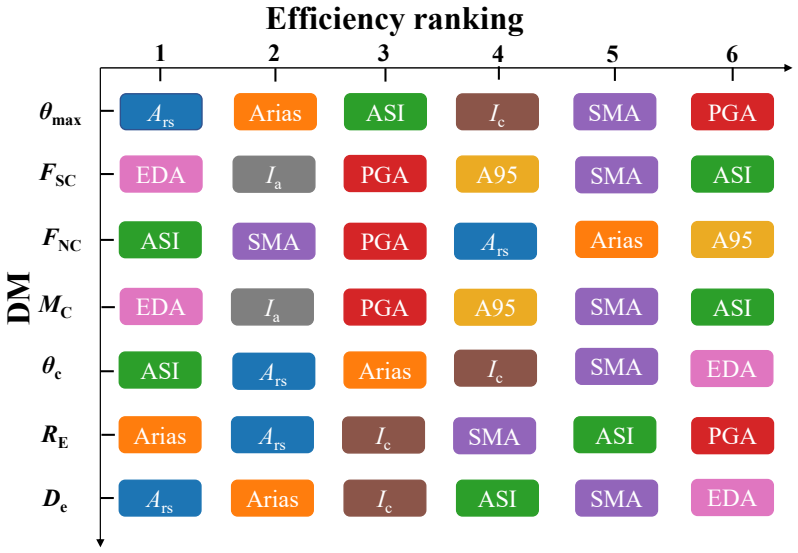


Figure 7. Efficiency ranking under different DMs.

5.2. Practicality Assessment

In line with Equation (3), a regression analysis is performed on the chosen 32 IMs and seven DMs. Figure 8 illustrates the regression coefficient (b) corresponding to each IM and DM. The data indicate that b remains relatively stable when varying the IM parameters for a given DM. Among the DMs, θ_{max}, θ_c, and D_e exhibit higher practicality levels. Conversely, R_E, F_{NC}, F_{SC}, and M_C score lower in terms of practicality, a finding that opposes their efficiency standings. Therefore, a comprehensive assessment of DMs via other metrics is essential to yield sensible DM parameters. To extend the discussion on IM practicality, Figure 9 presents the b values for each IM when D_e is employed as the DM. The analysis reveals that acceleration-type and spectral-type IMs have higher b values with less variability, thus indicating superior practicality. In contrast, displacement-type IMs are less practical. An overarching comparison of b values across various IMs under each DM is provided in Figure 10. This comparison leads to the conclusion that the most practical IMs are I_v, I_a, PGA, SMA, ASI, and A95.

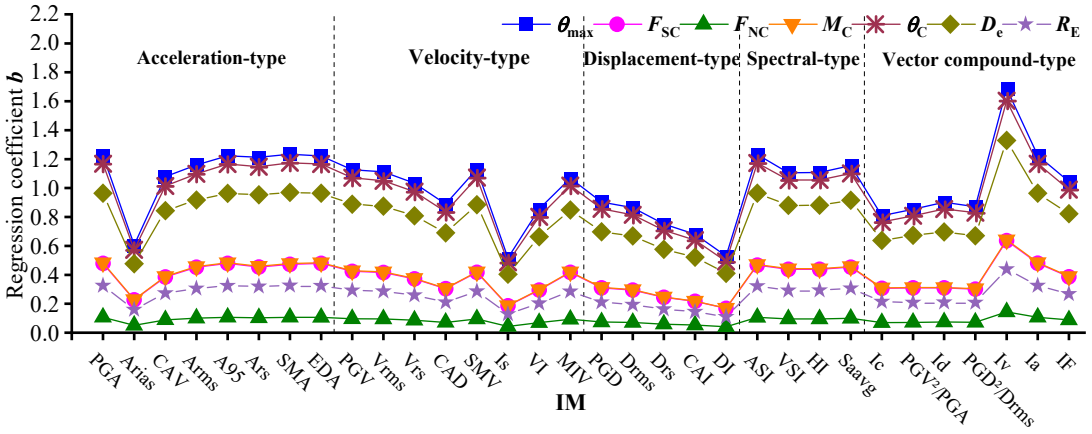


Figure 8. The value of b with different IMs and DMs.

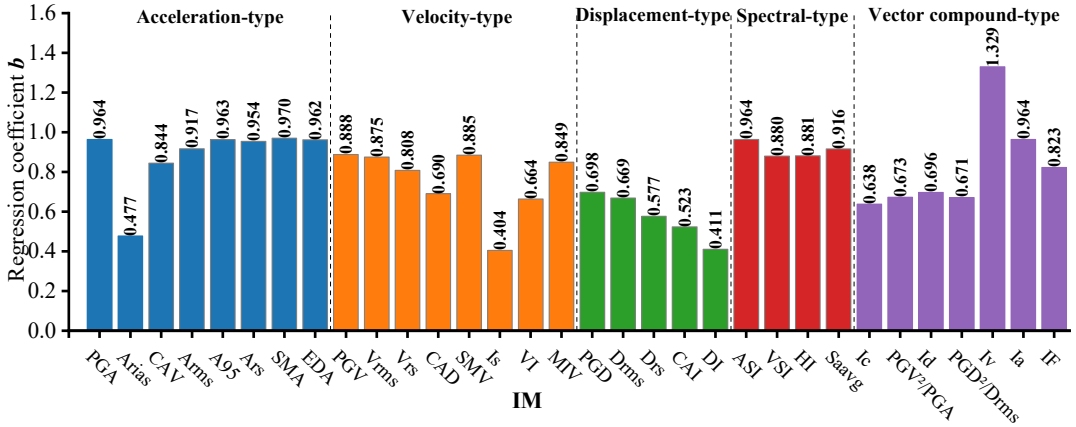


Figure 9. The value of b under each IM with D_e as the DM.

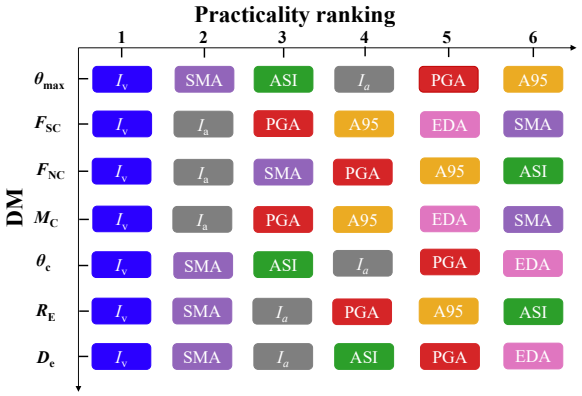


Figure 10. Practicality ranking under different DMs.

5.3. Proficiency Examination

When the metrics for efficiency and practicality yield conflicting results, proficiency serves as a composite metric to mitigate evaluation uncertainties. Figure 11 illustrates the proficiency values (ζ) corresponding to each IM and DM. A lower ζ value indicates higher proficiency. The results demonstrate that when each DM employs different IM parameters, the variation in ζ remains consistent. DMs such as θ_{max}, θ_c, D_e, and F_{NC} exhibit superior proficiency. Conversely, R_E, F_{SC}, and M_C rank lower in terms of proficiency. For a more nuanced comparison of IM proficiency, Figure 12 presents ζ values for each IM when R_E is utilized as the DM. It becomes evident that spectral-type IMs display lower ζ values, signifying higher proficiency. This is followed by velocity-type and acceleration-type IMs.

On the contrary, vector compound-type IMs manifest significant fluctuations in ζ and poor proficiency, and displacement-type IMs demonstrate the least proficiency. A detailed analysis of ζ values across different IMs for each DM is depicted in Figure 13, which reveals that the IMs with higher proficiency include I_v, I_a, PGA, SMA, and ASI. Furthermore, IMs with low proficiency are displacement-type IMs, especially DI and CAI.

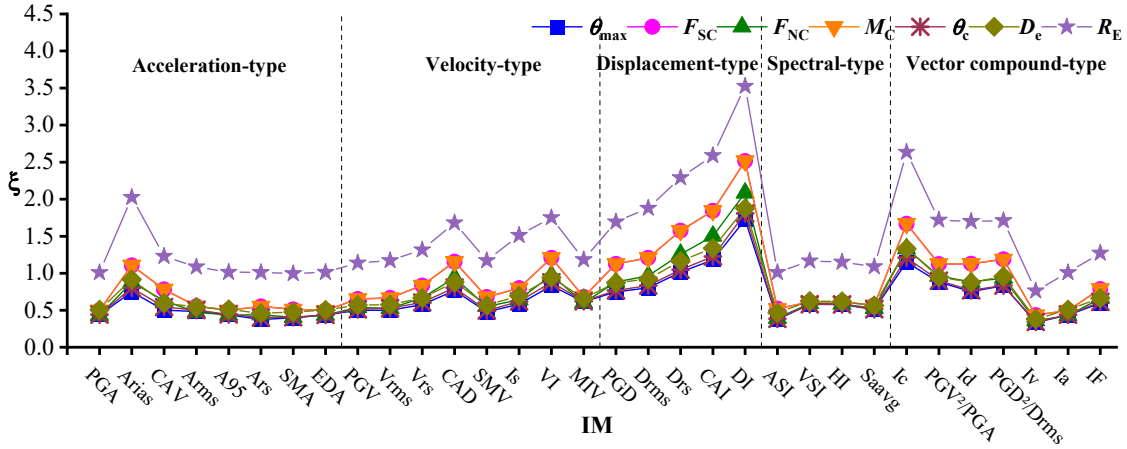


Figure 11. The value of ζ with different IMs and DMs.

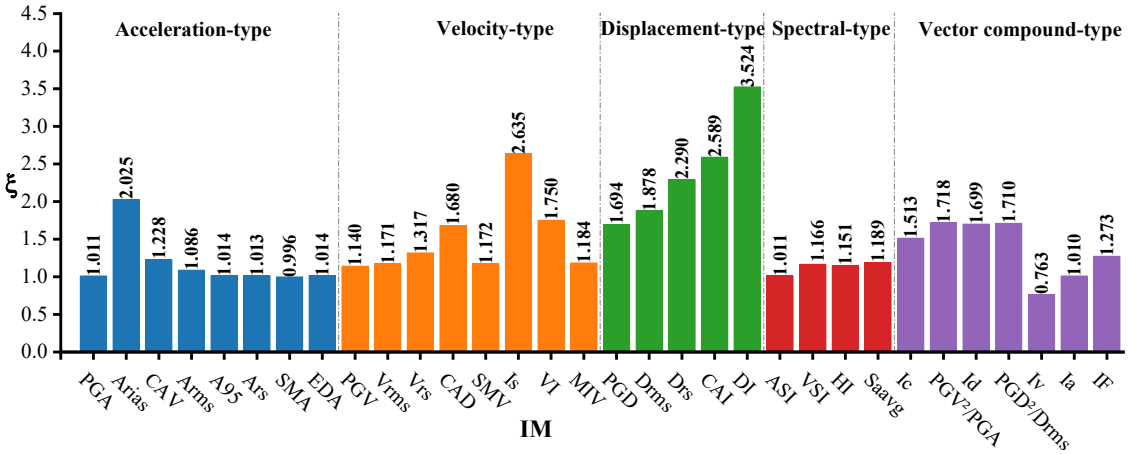


Figure 12. The value of ζ under each IM with R_E as the DM.

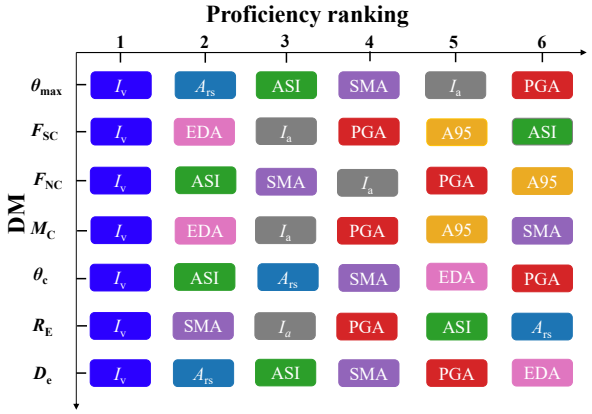
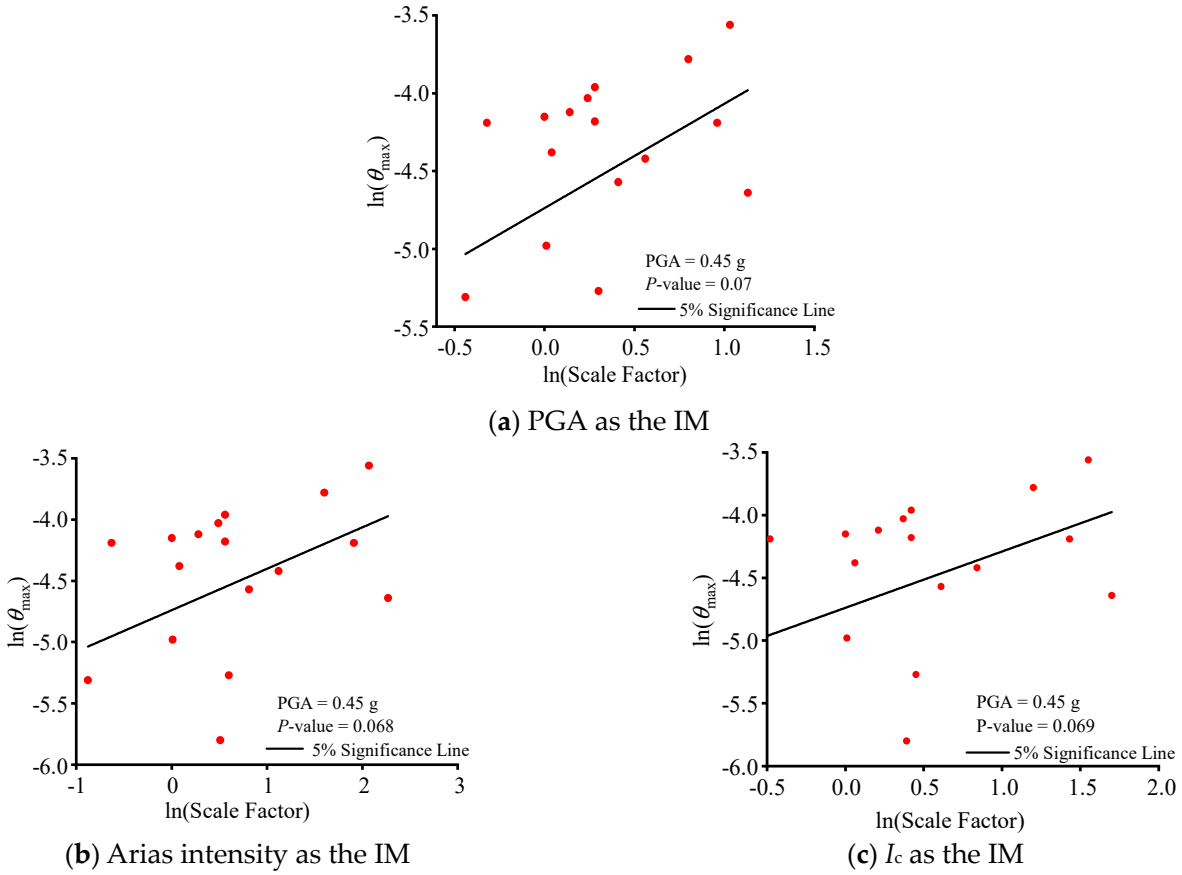


Figure 13. Proficiency ranking under different DMs.

5.4. Scaling Robustness Analysis

In compliance with the fitting methodology delineated in Section 3.4, this section examines the scaling robustness of PGA, Arias intensity, and I_c. Since the scaling factors

for other IMs remain constant, they are excluded from this analysis. Based on numerical simulations, when PGA exceeds or is equal to 0.5 g, the structural compression damage output, as simulated in ABAQUS, surpasses 0.9 and accelerates with increasing ground motion intensity. This phenomenon weakens the independence between DM and the scaling factor, making it challenging to evaluate the scaling robustness of IMs. Therefore, this section confines the investigation to a range of 0.03 g to 0.45 g for each IM. Figure 14 presents a regression analysis plot of the natural logarithm of ln(θ_{max}) and ln(Scale Factor) corresponding to PGA, Arias intensity, and I_c. At a PGA of 0.45 g, the *p*-values for these IMs are 0.07, 0.068, and 0.069, respectively—all exceeding the 0.05 threshold. To provide a comprehensive view of how *p*-values change with IM amplitude modulation, Table 4 lists the *p*-values for the three IMs at PGA levels ranging from 0.03 g to 0.45 g. Notably, all the *p*-values surpass 0.05, confirming that the selected IMs satisfy the criteria for scaling robustness, and the structural dynamic response is minimally affected by the ground motion scaling factor.



(**a**) PGA as the IM

(**b**) Arias intensity as the IM

(**c**) I_c as the IM

Figure 14. Regression analysis of ln(θ_{max}) and ln(Scale Factor).

Table 4. *p*-value of different IMs.

Modulation PGA (g)	0.03	0.06	0.1	0.15	0.2	0.25	0.3	0.35	0.4	0.45
PGA	0.391	0.205	0.063	0.654	0.327	0.178	0.199	0.063	0.063	0.07
Arias intensity	0.390	0.202	0.062	0.654	0.326	0.173	0.193	0.063	0.062	0.068
I_c	0.388	0.203	0.061	0.653	0.281	0.145	0.190	0.062	0.063	0.069

5.5. Relativity Insights

The relativity between IMs and DMs was quantitatively assessed using the statistical correlation coefficient R^2. Figure 15 provides a visualization of R^2 values across different IMs and DMs. The trend in R^2 remains substantially consistent irrespective of the specific

DMs and IMs considered. However, the relativity between R_E and each IM is notably weak, as evidenced by the lower R^2 values. Conversely, the remaining six types of DM exhibit higher correlation coefficients with each IM. To delve further into IM relativity, Figure 16 displays the variations in R^2 values when θ_{max} is employed as the DM. It becomes evident that displacement-type IMs exhibit a weak correlation with θ_{max} ($R^2 < 0.7$), while Arias intensity, EDA, PGA, A_{rs}, SMA, ASI, SMV, I_a, and I_c are all highly correlated ($R^2 > 0.8$). A comprehensive comparison of R^2 values across various IMs for each DM is illustrated in Figure 17. It becomes apparent that Arias intensity, A_{rs}, PGA, ASI, SMA, and I_c all exhibit high levels of correlation with each DM.

In terms of the relativity between IMs, the analysis focused on PGA due to the large number of IMs included in this study. As Figure 18 demonstrates, acceleration-type, spectral-type, and vector compound-type IMs exhibit a strong relativity with PGA. They are followed by velocity-type and displacement-type IMs. This suggests that if PGA is deemed suitable for the seismic performance analysis of a structure, then other IMs that are highly correlated with PGA will likewise be effective. Furthermore, a scrutiny of the R^2 values corresponding to each IM reveals that acceleration-type IMs have a particularly strong relativity with PGA. Similar trends are observed among other types of IMs; namely, the relativity is strong between IMs of the same type but weakens when different types of IMs are compared. If the correlation between IMs is weak, it is recommended to use the concept of relative adequacy of sufficiency as a criterion for judgment.

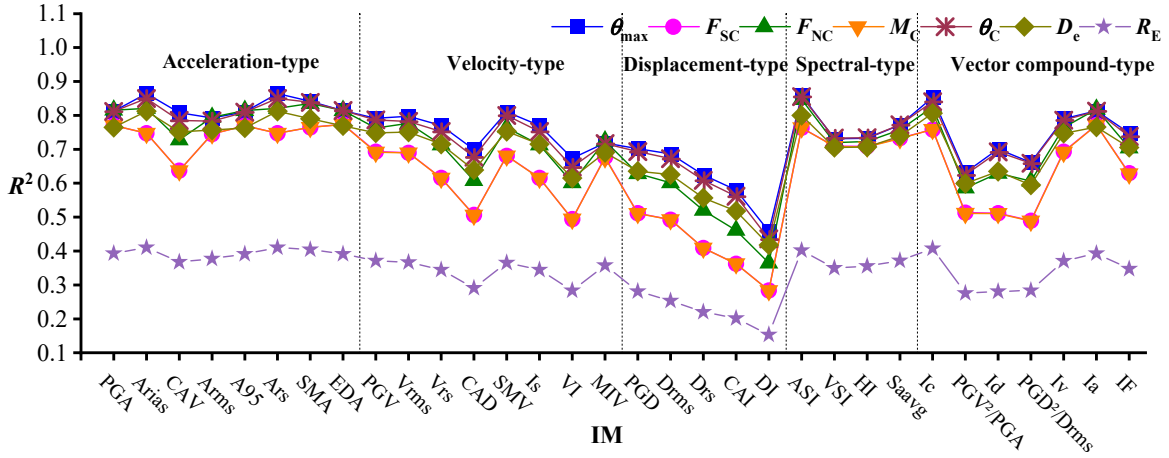


Figure 15. The value of R^2 with different IMs and DMs.

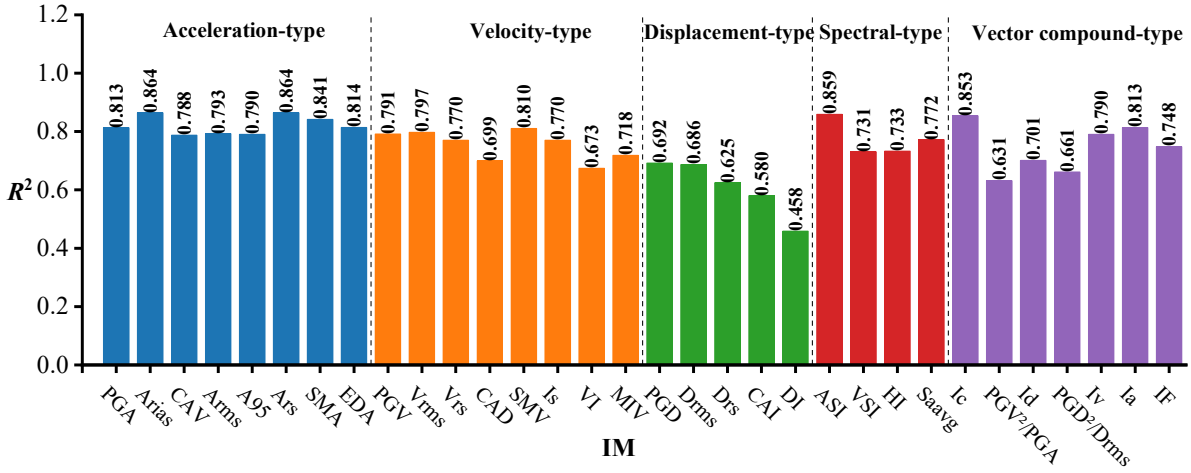


Figure 16. The value of R^2 under each IM with θ_{max} as the DM.

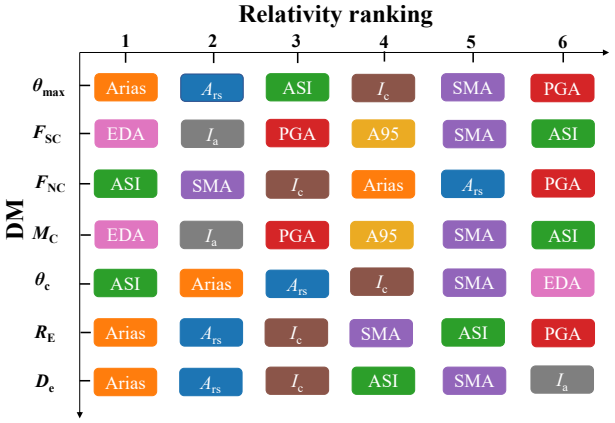


Figure 17. Relativity ranking under different DMs.

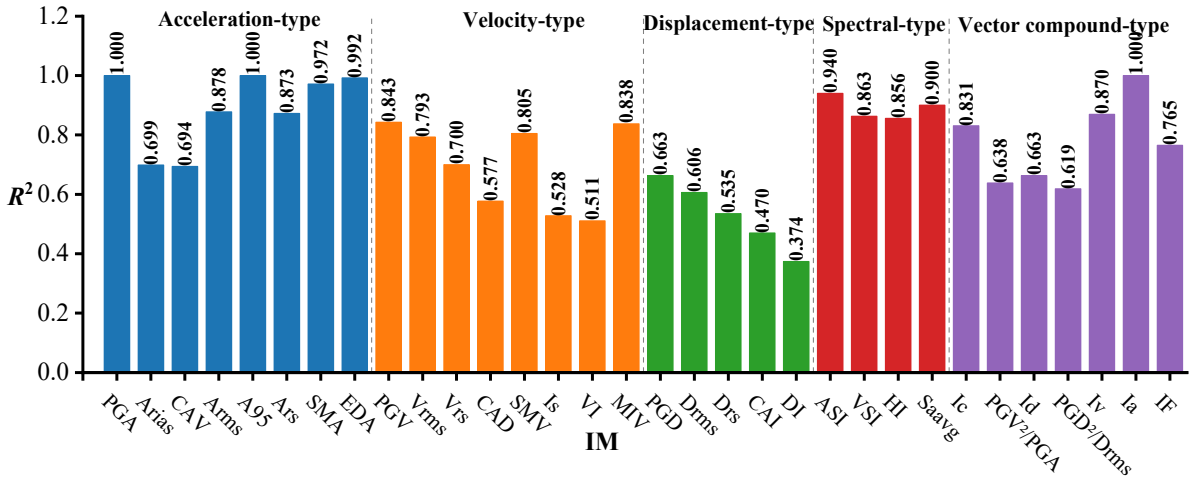


Figure 18. The value of R^2 under each IM.

5.6. Hazard Computability Evaluation

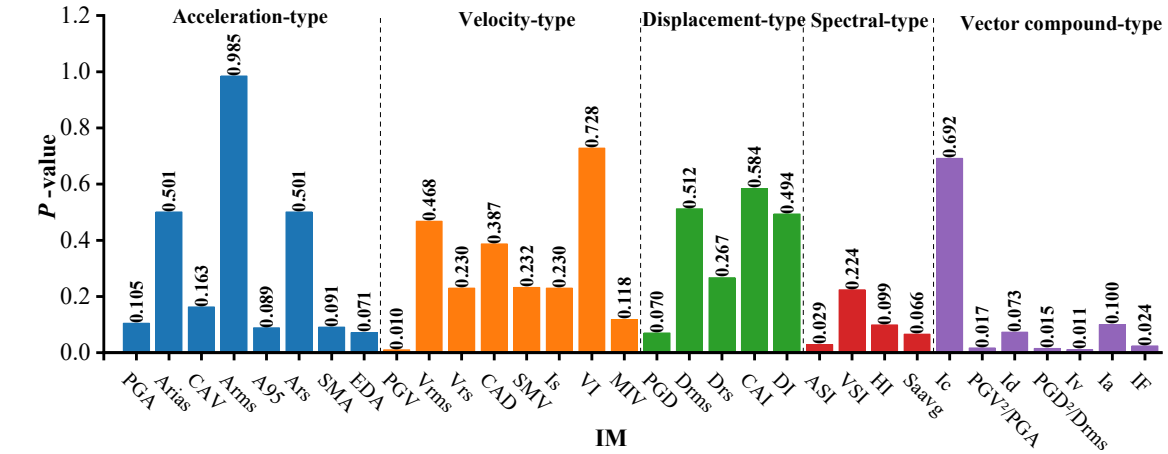
As described in Section 3.6, hazard computability assesses the likelihood of structural damage over varying years and evaluates the simplicity of computational procedures. Currently, PGA and S_a emerge as the IMs with superior hazard computability. The latest report from the United States' National Seismic Hazard Model (NSHM) [39] employs hazard curves to convey the 2%, 5%, and 10% exceedance probabilities for specific geographic regions over a 50-year span. The generation of these hazard curves relies on two pivotal factors: long-term seismic data and an abundant probability correction model. Within the United States Geological Survey (USGS) database [40], hazard calculations for PGA, PGV, peak ground displacement (PGD), and S_a are readily available and have been applied to various regions within the United States. For the area surrounding the Daikai station, which is the focus of this study, no hazard computation data are available. The absence of adequate earthquake data and a reliable probability correction model for this specific region necessitates the accumulation of such data for a nuanced understanding of hazard computability for different IMs.

Moreover, the hazard computability of multiple IMs can be inferred through their relativity with PGA. Employing Bradley's method [41], hazard curves for other IM types can be extrapolated from the existing IM hazard curve, as illustrated in Equation (8). As observed in Section 5.5, IMs such as A95, SMA, EDA, and I_a exhibit high relativity with PGA. The hazard curves for these correlated IMs can thus be derived through Equation (8) once a reliable PGA hazard curve is established.

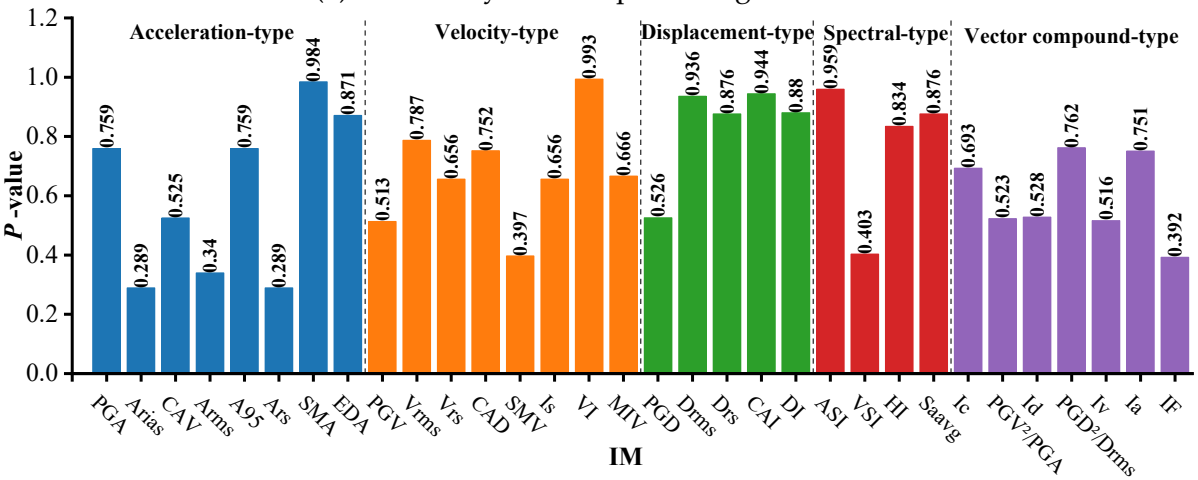
$$\lambda(IM_2) = \int_{IM} P[IM_2 \geq im_2 | IM_1] \cdot |d\lambda(IM_1)| \tag{8}$$

5.7. Sufficiency Analysis

The analysis of sufficiency, as described in Section 3.7, is visually represented in Figure 19, which plots IM sufficiency in relation to site conditions using θ_{max} as the DM, incorporating both earthquake magnitude and fault distance. Figure 19a reveals that 78% of the selected IMs adequately meet the criteria for magnitude sufficiency. Notably, A_{rms}, VI, I_c, D_{rms}, and CAI display enhanced magnitude sufficiency, whereas vector compound-type IMs lag behind in this regard. Figure 19b confirms that all IMs satisfy the fault distance sufficiency criteria.



(**a**) Sufficiency of earthquake magnitude *M*w



(**b**) Sufficiency of fault distance *R*

Figure 19. Sufficiency of site conditions.

In terms of the sufficiency between IMs, values of *I* for each IM are calculated using Equation (7) and are depicted in Figure 20. The figure highlights IMs with excellent and poor sufficiency, including A_{rs}, ASI, PGD, and DI. A_{rs} manifests better sufficiency, as evidenced by consistently positive *I* values, followed by ASI. Conversely, DI shows negative *I* values (except for self-comparison), indicating its limited sufficiency relative to other IMs. Similarly, PGD also exhibits reduced sufficiency. Overall, the analysis reveals that A_{rs}, ASI, I_c, PGA, and SMA possess greater sufficiency, whereas displacement-type IMs generally demonstrate inferior sufficiency.

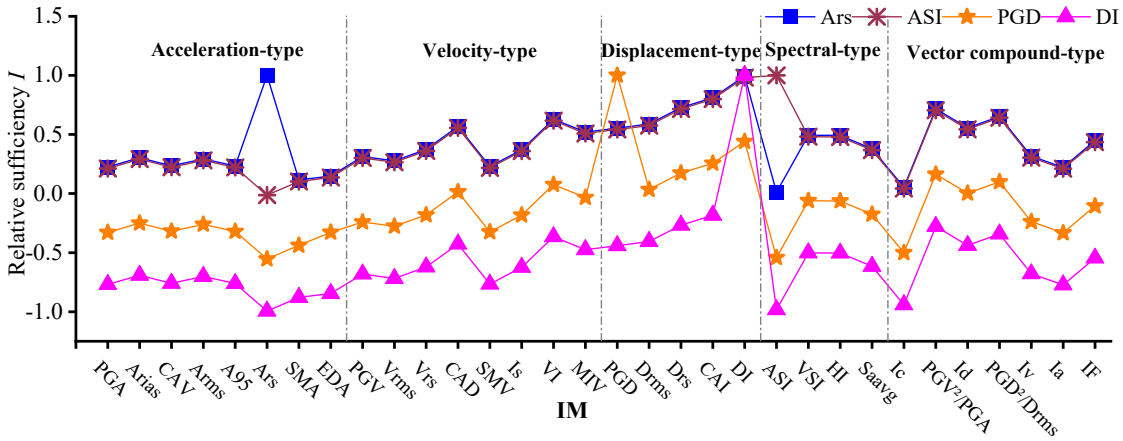


Figure 20. Sufficiency between IMs.

6. Measure Optimization Approach

Drawing upon the findings of our analysis, the optimal choice of DMs is influenced by four key criteria: efficiency, practicality, proficiency, and relativity. It is worth noting that the assessments of efficiency and practicality can be skewed due to the dimensional attributes of the DM, thereby leading to inconsistencies in the evaluation outcomes for these criteria. This issue is mitigated through the use of ζ, a dimensionless parameter, in proficiency analysis. Additionally, relativity serves as a robust measure of the linear association between IMs and DMs, thereby acting as a compensatory factor for the aforementioned limitations. Consequently, the optimal selection of an optimal DM is determined by considering both proficiency and relativity, in addition to efficiency and practicality.

When it comes to choosing an ideal IM, three primary requirements must be met: scaling robustness, hazard computability, and site-specific sufficiency. Specifically, scaling robustness ensures that the IM will not disproportionately influence the structural response during amplitude modulation. Meeting the hazard computability criterion allows for a more streamlined seismic analysis, facilitating the derivation of a precise seismic hazard curve with minimal computational effort. Finally, fulfilling the site-specific sufficiency criterion guarantees that variations in earthquake magnitude and fault distance will not compromise the analytical results.

In the context of IM selection, the pillars of efficiency, practicality, and proficiency serve as central guiding principles. The chosen IMs can be further verified through their relativity and relative sufficiency compared to other IMs. According to the analysis results of this study, the IMs selected based on efficiency, practicality, and proficiency remain basically the same, and also present higher relativity and relative sufficiency.

7. Conclusions

In this study, a two-dimensional finite element model of soil and structure was established using ABAQUS finite element software based on the Daikai subway station. IDA was executed on the structure with pulse-like ground motion records, incorporating 32 ground motion IMs spanning five categories and seven structural DMs covering three categories. Comprehensive analysis led to the identification of optimal IMs and DMs, thereby providing a foundational framework for the performance-based seismic design of underground structures. The principal conclusions can be summarized as follows:

- According to the seven properties of measure optimization, the optimal selection of DMs should be rigorously assessed based on efficiency, practicality, proficiency, and relativity. The IMs, on the other hand, should fulfill criteria such as scaling robustness, hazard computability, and site-specific sufficiency. In terms of IM optimization, efficiency, practicality, and proficiency stand as the cornerstone criteria, enhanced by relativity and relative sufficiency to validate the selected measures.

- For the shallow-buried subway station structure investigated in this study, DM optimization was performed using the criteria of efficiency, practicality, proficiency, and relativity. The parameters θ_{max}, θ_c, and D_e emerge as highly effective in capturing the damage state of underground structures, and their use is thus recommended.
- All 32 IMs examined in this study meet the standards of scaling robustness and sufficiency with respect to fault distance. Furthermore, 78% of the selected IMs comply with the criterion of sufficiency to magnitude. However, due to the absence of comprehensive seismic disaster data and probability correction models, the hazard computability of IM could not be definitively established, though specific implementation procedures were proposed.
- In the context of the shallow-buried subway station examined, the IMs were optimized using the criteria of efficiency, practicality, and proficiency. The metrics PGA, ASI, and SMA were found to be highly effective in characterizing ground motion intensity and exhibited superior relativity and relative sufficiency.

This article presents the optimal selection measures for a subway station structure. Considering the complexity of the pulse-like ground motions [36], future studies should focus on the influence of the pulse period on measure optimization to eliminate these limitations. Moreover, the conclusions drawn here are all based on the Daikai subway station's context. Therefore, subsequent studies should investigate the measure optimization for different structural forms to enhance the universality of IMs and DMs in the seismic analysis of underground structures. Additionally, the seismic hazard of the region is a crucial factor in selecting ground motion records [34]. Due to the lack of geological exploration and earthquake damage data, the selection of seismic ground motions was primarily based on site type, without considering the impact of seismic risk. This issue will be further improved in subsequent studies. Finally, due to limitations in seismic disaster data and the probability correction model, only specific implementation procedures were proposed. The specific calculation of the hazard computability of IMs should be addressed in our future research [42].

Author Contributions: Conceptualization, T.L. and Q.W.; methodology, T.L. and Y.H.; software, Y.H.; validation, T.L., Y.H. and Q.W.; investigation, T.L., Q.W. and Y.Y.; resources, T.L. and Y.Y.; writing—original draft preparation, Y.H.; writing—review and editing, T.L. and Q.W.; project administration, T.L. and Q.W. All authors have read and agreed to the published version of the manuscript.

Funding: This work was supported by the Liaoning Doctoral Scientific Research Foundation of China (2021-BS-165), the Liaoning Research Project of China (LJKMZ20220926), and the National Natural Science Foundation of China (52061135112), Liaoning Revitalization Talents Program (XLYC2203004).

Institutional Review Board Statement: Not applicable.

Informed Consent Statement: Not applicable.

Data Availability Statement: The data presented in this study are available in this article.

Acknowledgments: All support is gratefully acknowledged.

Conflicts of Interest: The authors declare no conflict of interest.

Appendix A. Intensity Measures Selected in This Study

Table A1. Acceleration type.

No.	Name	Definition
1	Peak ground acceleration	$PGA = \max\|a(t)\|$
2	Arias intensity	$I_A = \frac{\pi}{2g}\int_0^{T_{tot}}[a(t)]^2 dt$

Table A1. *Cont.*

No.	Name	Definition
3	Cumulative Absolute Velocity	$\mathrm{CAV} = \int_0^{T_{\mathrm{tot}}} \lvert a(t) \rvert dt$
4	Root Mean Square Acceleration	$A_{\mathrm{rms}} = \sqrt{\frac{1}{T_{\mathrm{d}}} \int_0^{T_{\mathrm{d}}} [a(t)]^2 dt}$
5	A95 Acceleration	The I_{A} corresponding to the part of ground motion time history less than A95 is 95% of the I_{A} of the whole ground motion time history
6	Root Mean Square Acceleration Integral	$A_{\mathrm{rs}} = \sqrt{E_a} \qquad E_a = \int_0^{T_{\mathrm{tot}}} a(t)^2 dt$
7	Sustained maximum acceleration	SMA: Maximum acceleration that can be maintained in three cycles of a ground motion time history
8	Effective Design Acceleration	EDA: Maximum acceleration of time history response filtered by a low-frequency 9 HZ filter

Table A2. Velocity type.

No.	Name	Definition
9	Peak ground velocity	$\mathrm{PGV} = \max \lvert v(t) \rvert$
10	Root Mean Square Velocity	$V_{\mathrm{rms}} = \sqrt{\frac{1}{T_d} \int_0^{T_{\mathrm{d}}} [v(t)]^2 dt}$
11	Root Mean Square Velocity Integral	$V_{\mathrm{rs}} = \sqrt{E_{\mathrm{V}}} \qquad E_{\mathrm{V}} = \int_0^{T_{\mathrm{tot}}} V(t)^2 dt$
12	Cumulative Absolute Displacement	$\mathrm{CAD} = \int_0^{T_{\mathrm{tot}}} \lvert v(t) \rvert dt$
13	Sustained Maximum Velocity	SMV: Maximum velocity that can be maintained during three cycles in a seismic time history
14	Specific Energy Density	$I_{\mathrm{S}} = \int_0^{T_{\mathrm{tot}}} [v(t)]^2 dt$
15	Velocity Intensity	$\mathrm{VI} = \frac{1}{\mathrm{PGV}} \int_0^{T_{\mathrm{d}}} [v(t)]^2 dt$
16	Maximum Incremental Velocity	MIV: Increment of velocity change

Table A3. Displacement type.

No.	Name	Definition
17	Peak ground displacement	$\mathrm{PGD} = \max \lvert d(t) \rvert$
18	Root Mean Square Displacement	$D_{rms} = \sqrt{\frac{1}{T_{\mathrm{d}}} \int_0^{T_{\mathrm{d}}} [d(t)]^2 dt}$
19	Root Mean Square Displacement Integral	$D_{\mathrm{rs}} = \sqrt{E_{\mathrm{D}}} \qquad E_{\mathrm{D}} = \int_0^{T_{\mathrm{tot}}} d(t)^2 dt$
20	Cumulative Absolute Impulse	$\mathrm{CAI} = \int_0^{T_{\mathrm{tot}}} \lvert d(t) \rvert dt$
21	Displacement Intensity	$\mathrm{DI} = \frac{1}{\mathrm{PGD}} \int_0^{T_{\mathrm{d}}} [d(t)]^2 dt$

Table A4. Spectral type.

No.	Name	Definition
22	Acceleration spectrum intensity	$\mathrm{ASI} = \int_{0.1}^{0.5} Sa(\xi = 5\%, T)dT$
23	Velocity Spectrum Intensity	$\mathrm{VSI} = \int_{0.1}^{2.5} Sv(\xi = 5\%, T)dT$
24	Housner Spectral Intensity	$\mathrm{HI} = \int_{0.1}^{2.5} \mathrm{PS_V} dT$
25	Average Spectral Acceleration	$Sa_{avg}(\xi, T) = \frac{\sum_{i=1}^{n} Sa(\xi,T)}{n}$

Table A5. Vector compound type.

No.	Name	Definition
26	Characteristic Intensity	$I_\mathrm{C} = A_\mathrm{rms}^{1.5} T_\mathrm{d}^{0.5}$
27	Ratio of peak ground velocity square to peak ground acceleration	$\frac{\mathrm{PGV}^2}{\mathrm{PGA}}$
28	Compound Displacement	$I_\mathrm{d} = \mathrm{PGD} \cdot T_\mathrm{d}^{\frac{1}{3}}$
29	Ratio of peak ground displacement square to Root Mean Square Displacement	$\frac{\mathrm{PGD}^2}{D_\mathrm{rms}}$
30	Compound Velocity	$I_V = \mathrm{PGV}^{\frac{2}{3}} \cdot T_\mathrm{d}^{\frac{1}{3}}$
31	Compound Acceleration	$I_a = \mathrm{PGA} \cdot T_\mathrm{d}^{\frac{1}{3}}$
32	Fajfar Intensity	$I_F = \mathrm{PGV} \times T_\mathrm{d}^{0.25}$

References

1. Liu, T.; Chen, Z.; Yuan, Y.; Shao, X. Fragility analysis of a subway station structure by incremental dynamic analysis. *Adv. Struct. Eng.* **2017**, *20*, 1111–1124. [CrossRef]
2. Zhong, Z.; Shen, Y.; Zhao, M.; Li, L.; Du, X.; Hao, H. Seismic fragility assessment of the daikai subway station in layered soil. *Soil Dyn. Earthq. Eng.* **2020**, *132*, 106044. [CrossRef]
3. Zhuang, H.; Yang, J.; Chen, S.; Dong, Z.; Chen, G. Statistical numerical method for determining seismic performance and fragility of shallow-buried underground structure. *Tunneling Undergr. Space Technol.* **2021**, *116*, 104090. [CrossRef]
4. Xu, M.; Cui, C.; Li, J.; Wang, G.; Su, J.; Gao, L. Seismic vulnerability analysis of subway station embedded in saturated sand layers. *Eng. Mech.* **2021**, *38* (Suppl. S1), 252–258. [CrossRef]
5. Jiang, J.; El Nggar, H.; Xu, C.; Zhong, Z.; Du, X. Effect of ground motion characteristics on seismic fragility of subway station. *Soil Dyn. Earthq. Eng.* **2021**, *143*, 106618. [CrossRef]
6. Huang, Z.; Pitilkis, K.; Tsinidis, G.; Argyroudis, S.; Zhang, D.-M. Seismic vulnerability of circular tunnels in soft soil deposits: The case of Shanghai metropolitan system. *Tunn. Undergr. Space Technol.* **2020**, *98*, 103341. [CrossRef]
7. Zhang, C.; Zhong, Z.; Zhen, L.; Shen, Y.; Zhao, M. Seismic intensity measures for the damage evaluation of circular tunnels. *Eng. Mech.* **2021**, *38*, 100–108. [CrossRef]
8. Cui, Z.; Sheng, Q.; Leng, X. Performance-based seismic stability assessment of large underground cavern group with incremental dynamic analysis. *Chin. J. Rock Mech. Eng.* **2012**, *31*, 703–712. [CrossRef]
9. Chen, Z.; Wei, J. Correlation between ground motion parameters and lining damage indices for mountain tunnels. *Nat. Hazards* **2013**, *65*, 1683–1702. [CrossRef]
10. Kiani, A.; Torabi, M.; Mirhosseini, M.S. Intensity measures for the seismic response evaluation of buried steel pipelines under near-field pulse-like ground motions. *Earthq. Eng. Eng. Dyn.* **2019**, *18*, 914–931. [CrossRef]
11. Zhong, Z.; Shen, Y.; Zhen, L.; Zhang, C.; Zhao, M.; Du, X. Ground motion intensity measures and dynamic response indexes of metro station structures. *Chin. J. Geotech. Eng.* **2020**, *42*, 486–494. [CrossRef]
12. Gu, Y.; Qiu, S.; Xiong, M. Study on the correlation between ground motion intensity indexes and seismic response of underground utility tunnel. *Earthq. Eng. Eng. Dyn.* **2021**, *41*, 22–37. [CrossRef]
13. Huang, Z.; Pitilakis, K.; Argyroudis, S.; Tsinidis, G.; Zhang, D.M. Selection of optimal intensity measures for fragility assessment of circular tunnels in soft soil deposits. *Soil Dyn. Earthq. Eng.* **2021**, *145*, 106724. [CrossRef]
14. Jiang, J.; Xu, C.; Du, X.; Chen, G.; Xu, Z. Optimal indicator of earthquake intensity measures for underground frame structure seismic design of shallow-buried subway station. *Chin. J. Geotech. Eng.* **2022**, 1–9. Available online: http://kns.cnki.net/kcms/detail/32.1124.TU.20220808.1729.004.html (accessed on 16 November 2023).

15. Baker, J.W.; Cornell, C.A. A vector-valued ground motion intensity measure consisting of spectral acceleration and epsilon. *Earthq. Eng. Struct. Dyn.* **2005**, *34*, 1193–1217. [CrossRef]
16. Jiang, J.; Li, W.; El Naggar, M.H.; Zhao, Y.; Chen, G.; Du, X. Optimal earthquake intensity measure in probabilistic seismic demand models of underground subway station structure. *Tunn. Undergr. Space Technol.* **2024**, *146*, 105659. [CrossRef]
17. Chen, Z.Y.; Yu, W.; Liu, Z.Q. Construction and verification of composite intensity measure representing the overall damage of underground structures. *Umu Gongcheng Xuebao/China Civ. Eng. J.* **2024**, *57*, 23–33. [CrossRef]
18. *GB/T 51336-2018*; Standard for Seismic Design of Underground Structures. China Architecture & Building Press: Beijing, China, 2018.
19. Park, Y.J.; Ang, A.H.S.; Wen, Y.K. Seismic damage analysis of reinforced concrete buildings. *J. Struct. Eng.* **1985**, *111*, 740–757. [CrossRef]
20. Jiang, J.; Sun, J. Seismic damage model of brick structure. *Earthq. Eng. Eng. Dynanics* **1987**, *7*, 20–34. [CrossRef]
21. Ou, J.; Niu, D.; Wang, G. Fuzzy dynamical reliability analysis and design of nonlinear a seismic steel structures. *J. Harbin Univ. Civ. Eng. Archit.* **1991**, *24*, 9–20.
22. Cornell, C.A.; Jalayer, F.; Hamburger, R.O.; Foutch, D.A. Probabilistic basis for 2000 SAC federal emergency management agency steel moment frame guidelines. *J. Struct. Eng.* **2002**, *128*, 526–533. [CrossRef]
23. Luco, N.; Cornell, C.A. Structure-specific scalar intensity measures for near-source and ordinary earthquake ground motions. *Earthq. Spectra* **2007**, *23*, 357–392. [CrossRef]
24. Padgett, J.E.; Nielsong, B.G.; Desroches, S.R. Selection of optimal intensity measures in probabilistic seismic demand models of highway bridge portfolios. *Earthq. Eng. Struct. Dyn.* **2008**, *37*, 711–725. [CrossRef]
25. Shafieezadeh, A.; Ramanathan, K.; Padgett, J.E.; DesRoches, R. Fractional order intensity measures for probabilistic seismic demand modeling applied to highway bridges. *Earthq. Eng. Struct. Dyn.* **2012**, *41*, 391–409. [CrossRef]
26. Tothong, P.; Luco, N. Probabilistic seismic demand analysis using advanced ground motion intensity measures. *Earthq. Eng. Struct. Dyn.* **2007**, *36*, 1838–1859. [CrossRef]
27. Zhou, Y.; Li, M. State-of-the-art of intensity measures for incremental dynamic analysis. *Struct. Eng.* **2014**, *30*, 199–204. [CrossRef]
28. Giovenale, P.; Corell, C.A.; Esteva, L. Comparing the adequacy of alternative ground motion intensity measures for the estimation of structural responses. *Earthq. Eng. Struct. Dyn.* **2004**, *33*, 951–979. [CrossRef]
29. Jalayer, F.; Beck, L.; Zareian, F. Analyzing the sufficiency of alternative scalar and vector intensity measures of ground shaking based on information theory. *J. Eng. Mech.* **2012**, *138*, 307–316. [CrossRef]
30. Lubliner, J.; Oliver, J.; Oller, S.; Oñate, E. A plastic-damage model for concrete. *Int. J. Solids Struct.* **1989**, *25*, 299–326. [CrossRef]
31. Lee, J.H.; Fenves, G.L. Plastic-damage model for cyclic loading of concrete structures. *J. Eng. Mech.* **1998**, *124*, 892–900. [CrossRef]
32. Huo, H.; Bobet, A.; Fernández, G.; Ramírez, J. Load transfer mechanisms between underground structure and surrounding ground: Evaluation of the failure of the Daikai station. *J. Geotech. Geoenviron. Eng.* **2005**, *131*, 1522–1533. [CrossRef]
33. *Nehrp Recommended Seismic Provisions for New Buildings and Other Structures*; Building Seismic Safety Council of the National Institute of Building Sciences: Washington, DC, USA, 2020.
34. Shome, N.; Cornell, C.A. *Probabilistic Seismic Demand Analysis of Nonlinear Structures*; Report No. RMS-35. RMS Program; Stanford University: Stanford, CA, USA, 1999.
35. Chen, Z.; Chen, W.; Li, Y.; Yuan, Y. Shaking table test of a multi-story subway station under pulse-like ground motions. *Soil Dyn. Earthq. Eng.* **2016**, *82*, 111–122. [CrossRef]
36. Yaghmaei-Sabegh, S.; Jafari-Koucheh, E.; Ebrahimi-Aghabagher, M. Estimating the seismic response of nonlinear structures equipped with nonlinear viscous damper subjected to pulse-like ground records. *Structure* **2020**, *28*, 1915–1923. [CrossRef]
37. Shahi, S.K.; Baker, J.W. An efficient algorithm to identify strong-velocity pulses in multicomponent ground motions. *Bull Seism. Soc Am.* **2014**, *104*, 2456–2466. [CrossRef]
38. Pacific Earthquake Engineering Research Center. PEER NGA Strong Motion Database. Available online: https://peer.berkeley.edu/peer-strong-ground-motion-databases (accessed on 6 June 2024).
39. Shumway, A.M.; Petersen, M.D.; Powers, P.M.; Rezaeian, S.; Rukstales, K.S.; Clayton, B.S. The 2018 update of the us national seismic hazard model: Additional period and site class data. *Earthq. Spectra* **2020**, *37*, 1145–1161. [CrossRef]
40. USGS Earthquake Hazards Program. Available online: http://earthquake.usgs.gov/ (accessed on 6 June 2024).
41. Bradley, B.A. The seismic demand hazard and importance of the conditioning intensity measure. *Earthq. Eng. Struct. Dyn.* **2012**, *41*, 1417–1437. [CrossRef]
42. Ahmet, D.; Mehmet, P.; Ali, H.K. Evaluation the effect of amplitude scaling of real ground motions on seismic demands accounting different structural characteristics and soil classes. *Bull. Earthq. Eng.* **2023**, *22*, 365–393. [CrossRef]

Disclaimer/Publisher's Note: The statements, opinions and data contained in all publications are solely those of the individual author(s) and contributor(s) and not of MDPI and/or the editor(s). MDPI and/or the editor(s) disclaim responsibility for any injury to people or property resulting from any ideas, methods, instructions or products referred to in the content.